# Aerodynamic Evaluation of NACA 4415 and Kline-Fogleman Upward Stepped Airfoil Using ANSYS: A Study on Lift Characteristics and Stall Delay

**[1]Golla Sathvika, [2] Sreeya Nalluri, [3] Bhukya Santhosh, [4] K. Arun Kumar**

[1]Undergraduate Student , Department of Aeronautical Engineering.
[2]Undergraduate Student , Department of Aeronautical Engineering.
[3]Undergraduate Student , Department of Aeronautical Engineering.
[4]Assistant Professor, Department of Aeronautical Engineering
Institute of Aeronautical Engineering, Dundigal, Hyderabad-500043
[1]sathvikayadav45@gmail.com [2]sreeyanalluri14@gmail.com [3]bhukyasanthu9908@gmail.com [4]k.arunkumar@iare.ac.in

***Abstract*— This research predominantly focuses on the lift characteristics and stall mechanisms in Kline Fogleman (KFm-2) upward stepped airfoill, emphasizing its innovative geometry and investigating how it performs in comparison with the NACA 4415 developed by the National Advisory Committee for Aeronautics. The NACA 4415 and the Kline Fogleman Kfm-2 Airfoil are chosen for the research because of their contrasting Design features. While the NACA 4415 is a conventional benchmark, the Kfm-2 is an innovative configuration aimed at enhancing stall resistance. Stall delay is the ability of the airfoil to maintain lift at high angles of attack (AoA), preventing an abrupt loss of control The stepped geometry of the KFm-2 airfoil, featuring vortex-trapping notches, enhances stall delay and enables stable performance at high angles of attack. This makes it well-suited for applications such as UAVs, RC aircraft, micro air vehicles, and high-lift devices. Lift characteristics, such as maximum lift coefficient and lift curve have been studied at moderate subsonic speeds ranging from 0.3- 0.6 across angles of attack of 0°, 4°, 8°, 12°, and 16°, within a moderate Reynolds number regime. Flow separation has likewise been observed; nonetheless, the Kline–Fogleman airfoil exhibits an enhanced capacity to sustain attached flow at elevated angles of attack owing to its stepped geometry, which encourages vortex generation and postpones separation. ANSYS was utilized for the computational analysis. The results highlight the stall-delay behaviour exhibited by the KFm-2 Airfoil, showing better lift performance even at greater angles of attack and a more gradual approach to stall.***

***Index Terms*— KFm-2 airfoil, NACA 4415, stall delay, lift characteristics, CFD analysis, flow separation, high angle of attack, stepped airfoil geometry.**

## I. INTRODUCTION

It is important for one to know how the airfoil becomes the fundamental aspect to generate lift. The cross-sectional shape of a wing is called an airfoil. As the basic aerodynamic surfaces, they provide lift, control, and stability for aircraft wings, propellers, and turbines, becoming the cornerstone of aeronautical engineering. Lift arises primarily from the pressure difference between the upper and lower surfaces of an airfoil as air flows over it. Lift can vary according to several factors, including free-stream velocity, angle of attack (AOA), Flow Conditions, and airfoil characteristics. Airfoils are commonly categorised into two types: symmetric and cambered airfoils. Symmetric airfoils possess identical upper and lower surfaces and produce no lift at zero angle of attack. Cambered airfoils feature a curved profile, enabling lift generation even at zero angle of attack and yielding higher lift coefficients. In this study, we concentrate on cambered airfoils, using NACA 4415 as a representative example, since their curved geometry allows them to generate lift at zero angle of attack.

The boundary layer is the thin layer of air that flows close to the airfoil surface where viscous effects are crucial. As the AOA increases, the lift also increases as the pressure difference between the upper and lower surfaces of the airfoil is greater. Nevertheless, after a certain threshold, the airflow over the top surface encounters an adverse pressure gradient, where pressure

rises in the direction of the flow, causing the boundary layer to decelerate. At a specific angle of attack the boundary layer loses the sufficient momentum and starts to seperate from the surface. As the angle increases further, it spreads rapidly over the airfoil. This results in stall, where the airflow is severely disrupted, leading to a sharp decline in lift and increase in drag.

Stall delay marks a significant breakthrough in airfoil aerodynamics, describing an airfoil's ability to maintain lift at high angles of attack (AoA) even after conventional profiles would typically experience sudden flow separation and stall. Unlike traditional stall, which is characterized by an abrupt drop in lift coefficient due to boundary layer separation under strong adverse pressure gradients, stall delay allows for a more gradual reduction in lift. This effect, often achieved through geometric modifications such as the stepped configuration of the KFm-2 airfoil, significantly enhances aerodynamic stability, safety, and operational flexibility. From a fluid dynamics perspective, the delayed stall behaviour is closely associated with the formation of a stable recirculation zone near the step, which traps a vortex and continuously re-energizes the boundary layer. This interaction between high-momentum outer flow and low-momentum near-wall flow reduces the tendency for large-scale flow separation. As a result, the airfoil can sustain attached or partially attached flow even beyond the conventional critical angle of attack. The step effectively alters the local pressure gradient, weakening the adverse pressure rise over the upper surface and enabling smoother pressure recovery toward the trailing edge. As the angle of attack increases, the recirculation region intensifies and contributes to a controlled separation mechanism rather than a complete flow breakdown. This leads to a progressive transition from attached to separated flow, avoiding the sudden aerodynamic penalties typically associated with stall. The lift curve, therefore, exhibits a more gradual slope change near the critical region, enhancing predictability and control. Additionally, the vortex structure generated at the step acts as an energy buffer, stabilizing the flow against external disturbances such as gusts or rapid changes in operating conditions.

In practical applications, this characteristic becomes particularly valuable in low Reynolds number regimes, where flow separation is more dominant and detrimental. For UAVs, micro air vehicles (MAVs), and remotely piloted systems, the ability to maintain lift at higher AoA translates to improved manoeuvrability, better endurance, and enhanced payload stability. The delayed stall also allows for steeper climb and descent profiles without compromising lift, which is especially useful in constrained environments and short take-off and landing (STOL) operations. Furthermore, the comparative evaluation between the NACA 4415 and KFm-2 airfoils highlights a fundamental trade-off between peak lift performance and post-stall stability. While conventional airfoils like NACA 4415 are optimized for higher lift in the pre-stall region, they are more susceptible to sharp stall characteristics due to rapid boundary layer separation. In contrast, the KFm-2 airfoil may exhibit slightly lower maximum lift coefficients, but it compensates by sustaining lift at higher angles of attack. In effect, although the peak lift is lower, similar lift levels can still be achieved at higher AoA in a more gradual and stable manner due to delayed stall. This extended lift capability broadens the operational envelope of the airfoil, making it highly suitable for applications where robustness and controllability are prioritized over maximum aerodynamic efficiency. Additionally, the reduced sensitivity to flow separation makes the KFm-2 airfoil less dependent on precise operating conditions, thereby improving performance consistency across varying flight regimes. Overall, the incorporation of stall delay mechanisms represents a significant advancement in airfoil design, offering a balanced combination of stability, adaptability, and sustained aerodynamic performance.

## II. METHODOLOGY

The aerodynamic performance of the NACA 4415 and Kline–Fogleman upward stepped airfoils is assessed through computational fluid dynamics (CFD) simulations conducted in ANSYS 2024. The flow field is governed by the fundamental conservation equations of mass, momentum, and energy. The Reynolds-Averaged Navier–Stokes (RANS) equations, combined with a suitable turbulence model like the k–ε model using standard wall functions, are utilized to account for turbulence effects that play a crucial role in lift generation and delaying stall.

## Geometry Modelling and Meshing

The geometric designs of the NACA 4415 (Fig. 1:(a)) and Kline–Fogleman (Fig. 1:(b)) upward stepped airfoils are created by importing their respective coordinate data into Fusion 360. This process generates smooth surface profiles that accurately depict the airfoil shapes. The NACA 4415 airfoil is built according to its standard specifications, while the KFm-2 model is adapted by adding an upward step on the upper surface, located at about 50% of the chord length. The KFm-2 airfoil features a thickness between 7% and 9% of the chord, aligning with typical low-speed applications and incorporating the step to encourage vortex creation and delay flow separation. Introducing a small camber on the lower surface of the KFm-2 airfoil enhances its effective camber, leading to improved lift generation without significantly altering the upper surface flow structure. Geometrically, this modification provides a smoother pressure distribution and better load sharing across the airfoil, further supporting delayed stall and improved aerodynamic efficiency. For the CFD analysis, a C-shaped computational domain is established around each airfoil, with upstream and downstream lengths kept in a 3:2 ratio relative to the chord length as shown in Fig. 2:(b). This setup effectively captures inlet flow development and wake formation while reducing boundary effects.

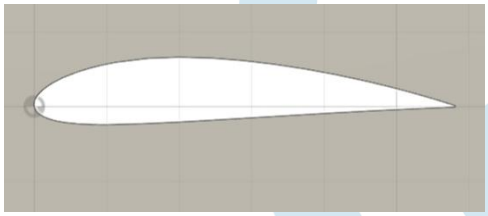

**Fig. 1:(a)** NACA 4415 airfoil

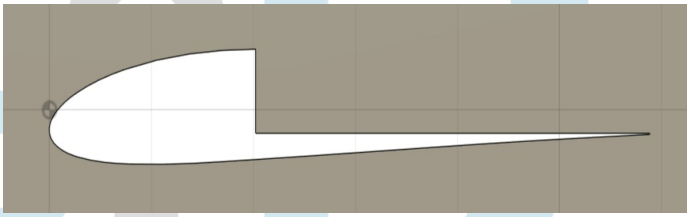

**Fig. 1:(b)** KFm-2 airfoil.

Once the geometry is finalized in the design software, it is transferred to ANSYS for meshing. An initial mesh is created using default settings and then refined to enhance solution accuracy. Mesh refinement involves applying edge sizing along the airfoil surface and critical areas, along with localized element size control to better resolve flow gradients. Additionally, inflation layers are added along the airfoil wall to accurately capture boundary layer behaviour, with careful management of growth rate and layer thickness. The near-wall resolution is maintained so that the first cell height corresponds to a $y^+$ value around $10^{-6}$ m, ensuring proper resolution of the viscous sublayer and improving turbulence modelling accuracy. This refined meshing strategy allows for precise prediction of flow separation, vortex formation, and stall characteristics for both airfoil designs.

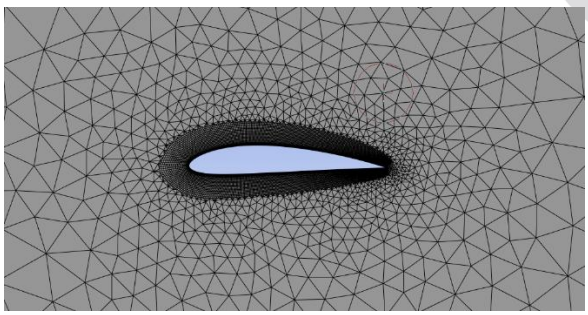

**Fig. 2:(a)** Mesh Configuration Of The NACA 4415

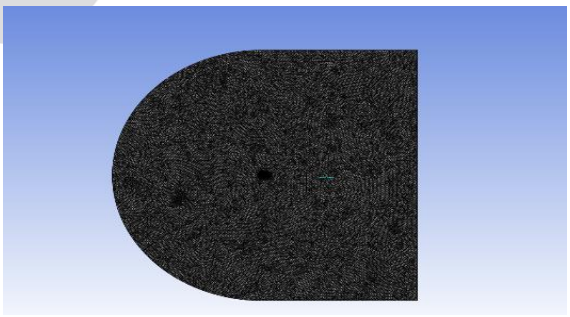

**Fig. 2:(b)** C-type domain

## Simulation Procedure

Simulations are conducted under steady, incompressible flow conditions across a range of attack angles from 0° to 16° in moderate Reynold's regime and subsonic speeds ranging from 0.3- 0.6, employing a suitable turbulence model like the k-omega SST to capture flow separation effects. For each angle of attack, the solution is iterated until it converges, and aerodynamic parameters

such as the lift coefficient are determined. The lift force is calculated using the below relation and is verified with the simulation results.

$$L = \frac{1}{2}\rho V^2 S C_L$$

Here $L$ is the lift force, $V$ is the freestream velocity, S is the frontal area and $C_L$ is the lift coefficient. The inlet is characterized as a velocity inlet corresponding to the selected Mach number, while the outlet is designated as a pressure outlet. A no-slip boundary condition is applied to the aerofoil surface to accurately simulate viscous effects, and the far-field boundaries are positioned far enough away to allow for undisturbed flow development. Then corresponding lift curves ($C_L$ vs α) are plotted to identify linear regions and stall points.

### Methodology-Based Validation

The present simulation framework has been developed and interpreted with reference to the methodology presented in [1] and [2], which provides a comprehensive numerical approach for analysing the aerodynamic behaviour of NACA 4415 and Kline-Fogleman airfoils.

## III. RESULTS AND DISCUSSIONS

The lift variation with angle of attack (AoA) for both airfoils across Mach numbers 0.3–0.6 reveals distinct aerodynamic behaviour in terms of lift generation and stall characteristics, as shown in **Fig. 3:(a)** and **Fig. 3:(b)**

For the KFm-2 airfoil the lift increases almost linearly with AoA for all Mach numbers, with no significant drop observed up to 16°. This indicates a delayed stall behaviour. As Mach number increases, the lift values increase substantially due to higher dynamic pressure, with the highest lift observed at M = 0.6. The absence of a sharp decline suggests that the KFm-2 maintains attached or controlled separated flow, likely due to vortex formation and recirculation near the step, which energizes the boundary layer and delays flow separation.

In contrast, the NACA 4415 airfoil shows a different trend. Lift increases with AoA up to around 12°, after which a clear drop in lift at 16° is observed for all Mach numbers. This indicates the occurrence of stall, where boundary layer separation becomes significant due to the adverse pressure gradient. Although the NACA 4415 produces higher lift than KFm-2 at lower AoA in some cases, its performance deteriorates beyond the critical angle of attack.

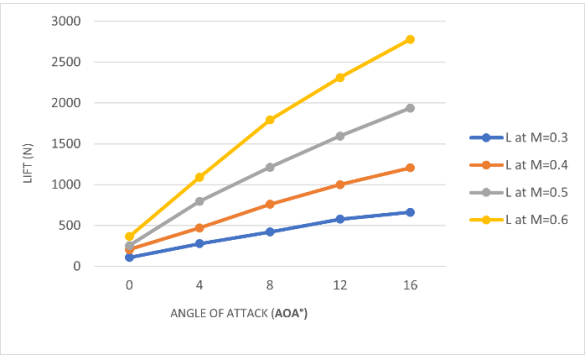


**Fig. 3:(a)** Variation of lift with angle of attack for different Mach numbers for the KFm-2 airfoil

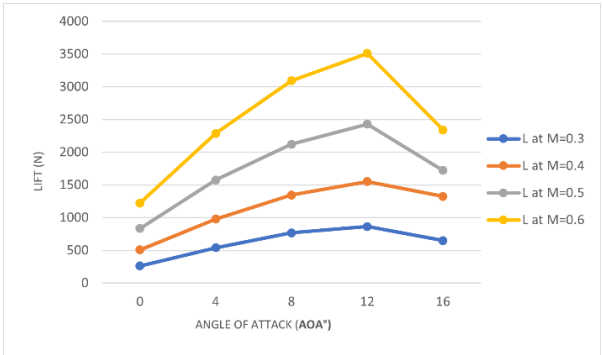


**Fig. 3:(b)** Variation of lift with angle of attack for different Mach numbers for the NACA 4415airfoil

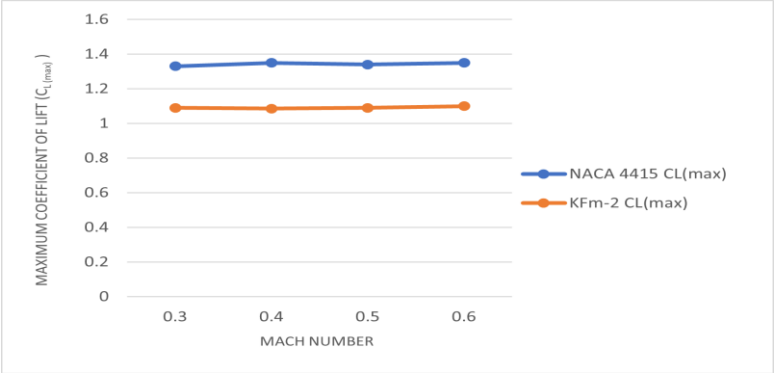


**Fig. 4:** Comparison of $C_{L(max)}$ with Mach number for NACA 4415 and KFm-2 airfoils.

For the NACA 4415 airfoil, the $C_{L(max)}$ remains consistently higher, with values around 1.33–1.36, showing only minor fluctuations with increasing Mach number. This indicates that the airfoil maintains strong lift-generating capability, but its maximum lift is constrained by earlier stall onset, as observed in previous plots. In contrast, the KFm-2 airfoil exhibits a lower $C_{L(max)}$ , approximately in the range of 1.08–1.15, but remains nearly constant across all Mach numbers. This consistency suggests that the aerodynamic performance of KFm-2 is less sensitive to Mach number variations within this regime. Although the NACA 4415 airfoil attains higher lift values in the pre-stall region, similar lift levels are achieved by the KFm-2 airfoil at higher angles of attack. This is due to its delayed stall characteristics, which allow it to sustain lift generation beyond the critical angle without abrupt flow separation. The variation of maximum lift coefficient with Mach number for both airfoils shows relatively stable behaviour across the subsonic range (M = 0.3 to 0.6) which is observed from Fig.4.

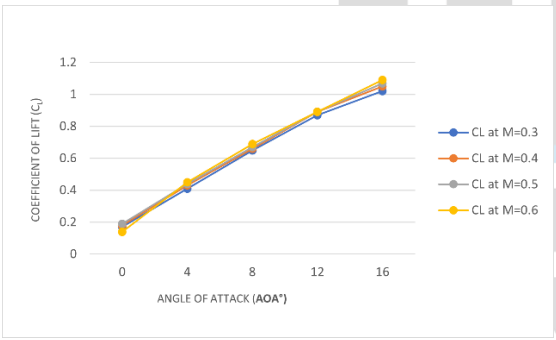


**Fig. 5:(a)** Variation of lift coefficient with angle of attack for different Mach numbers for the KFm-2 airfoil

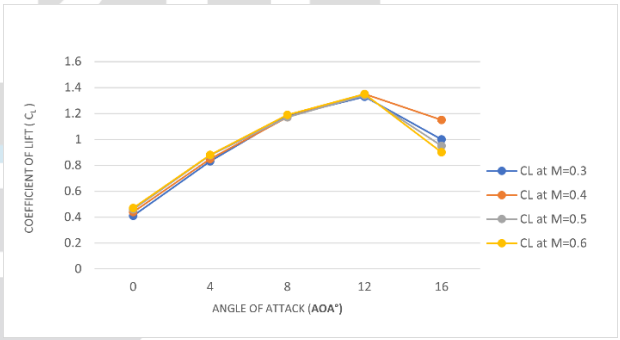


**Fig. 5:(b)** Variation of lift coefficient with angle of attack for different Mach numbers for the NACA 4415 airfoil

The $C_L$ vs angle of attack curves for both airfoils exhibit similar linear lift growth trends in the pre-stall region, with only marginal variation across Mach numbers, indicating minimal compressibility effects in this regime. The slope of the curves remains nearly consistent for both airfoils, suggesting comparable lift sensitivity to angle of attack initially. However, a key distinction arises near higher angles, where the NACA 4415 airfoil reaches its peak $C_L$ around 12° which is clearly observed in Fig.5:(b) and subsequently experiences a reduction, marking the onset of stall, whereas the KFm-2 airfoil continues its upward trend without any degradation which is observed in Fig.5:(a) . This reflects a shift not in lift slope but in lift sustainability beyond the critical angle. Although NACA 4415 achieves higher lift coefficients earlier, the KFm-2 compensates by extending the lift curve to higher angles, enabling it to attain similar lift levels progressively due to its delayed stall behavior. This highlights that the primary difference between the two lies not in initial lift generation, but in post-critical performance and stability.

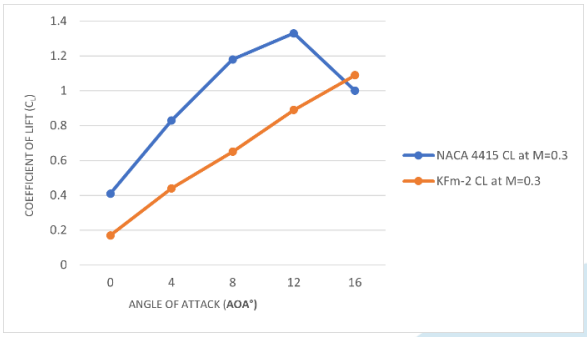


**Fig. 6:(a)** Comparison of Lift Coefficient and Angle of Attack at Mach 0.3 for KFm-2 and

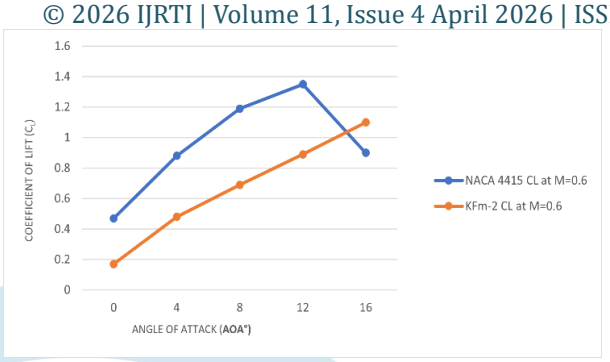


**Fig. 6:(b)** Comparison of Lift Coefficient and Angle of Attack at Mach 0.6 for KFm-2 and

The plots Fig.6(a) and Fig.6(b) show the variation of lift coefficient ($C_L$) with angle of attack at Mach 0.3 and Mach 0.6 for both NACA 4415 and KFm-2 airfoils.

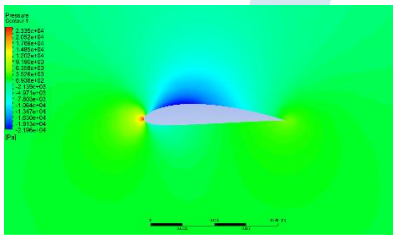

**Fig. 7:(a)** NACA 4415 at 0° AoA at Mach 0.6

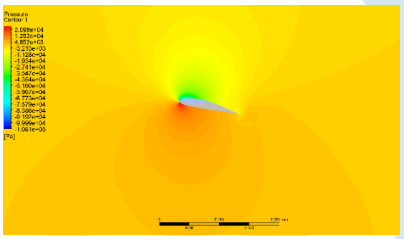

**Fig. 7:(b)** NACA 4415 at 12° AoA at Mach 0.6

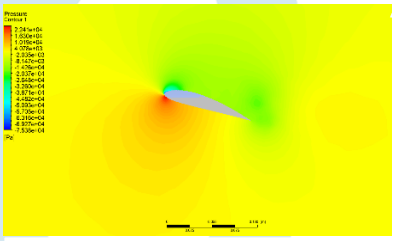

**Fig. 7:(c)** NACA 4415 at 16° AoA at Mach 0.6

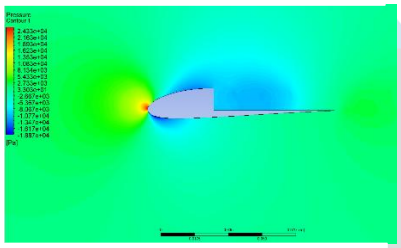

**Fig. 7:(d)** KFm-2 at 0° AoA at Mach 0.6

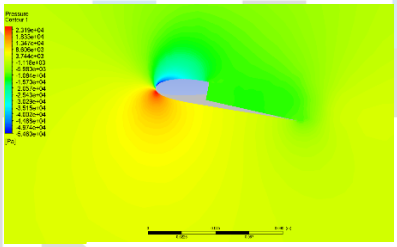

**Fig. 7:(e)** KFm-2 at 12° AoA Mach 0.6

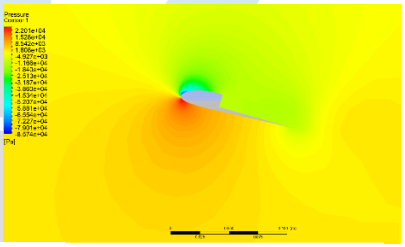

**Fig. 7:(f)** KFm-2 at 16° AoA at Mach 0.6

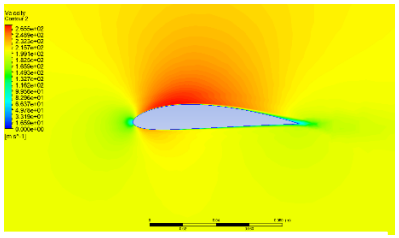

**Fig. 8:(a)** NACA 4415 at 0° AoA at Mach 0.6

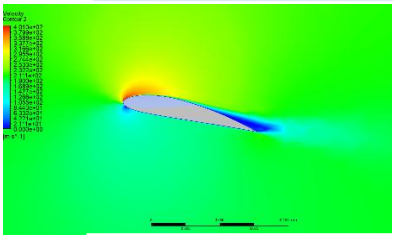

**Fig. 8:(b)** NACA 4415 at 12° AoA at Mach 0.6

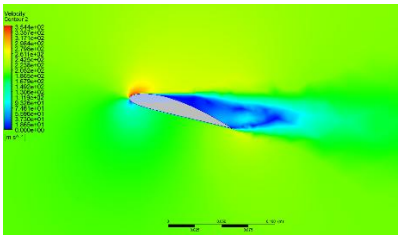

**Fig. 8:(c)** NACA 4415 at 16° AoA at Mach 0.6

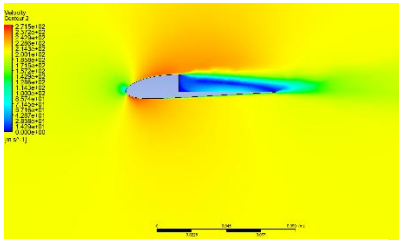

**Fig. 8:(d)** KFm-2 at 0° AoA at Mach 0.6

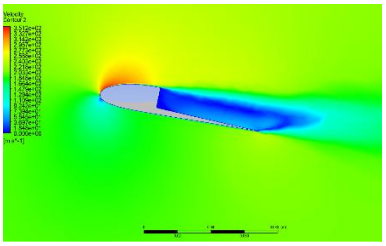

**Fig. 8:(e)** KFm-2 at 12° AoA at Mach 0.6

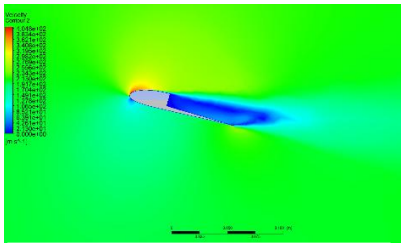

**Fig. 8:(f)** KFm-2 at 16° AoA at Mach 0.6

The static pressure contours Fig. 7:(a)-(f) and velocity contours Fig. 8:(a)-(f) obtained for the NACA 4415 and KFm-2 airfoils across angles of attack 0°, 12°, and 16° reveal a progressive evolution of the flow field, highlighting the role of the step in KFm-2 airfoil in modifying both pressure and velocity behavior. At 0° angle of attack, the pressure distribution is nearly symmetric, with the stagnation point near the leading edge. The velocity field remains uniform, with smooth acceleration over the upper

surface. A small disturbance near the step creates a mild pressure drop and a weak low-velocity recirculation zone, though the flow largely remains attached. At 0° angle of attack, the flow over a conventional smooth airfoil would typically remain fully attached as shown in Fig. 9:(a) with a symmetric pressure and velocity distribution. However, in the case of the KFm-2 airfoil, the presence of the step introduces a geometric discontinuity that alters the local flow behavior even at zero incidence. The recirculation region (**Fig. 9:(b)**) initiates just downstream of the step due to an abrupt change in surface geometry, which causes a localized flow separation. As the boundary layer encounters the step, it is unable to follow the sudden contour change, leading to a small separation bubble. This results in the formation of a low-velocity recirculating zone near the upper surface behind the step. The outer flow continues to move smoothly over this region, creating a shear layer between the high-speed freestream and the slower recirculating flow beneath it. At this stage, the recirculation zone is weak, small in size, and stable, and does not significantly affect the overall aerodynamic performance. Instead, it plays a preparatory role by establishing a vortex-trapping mechanism, which becomes more influential at higher angles of attack

Building on the weak recirculation observed at 0°, the flow behavior becomes more pronounced at 12° angle of attack. The stagnation point shifts downward along the lower surface, increasing the pressure difference across the airfoil. A strong low-pressure region forms near the step on the upper surface, accompanied by high flow acceleration followed by a clearly defined low-velocity recirculation zone. At this stage, the recirculation region develops into a **controlled separation bubble**, with a sharp velocity gradient between the outer flow and the recirculating region. This interaction energizes the boundary layer and delays large-scale separation. As a result, pressure recovery becomes more gradual, and the wake elongates while remaining relatively organized. The initially weak recirculation thus evolves into an important flow-control mechanism that stabilizes the flow at higher angles of attack.

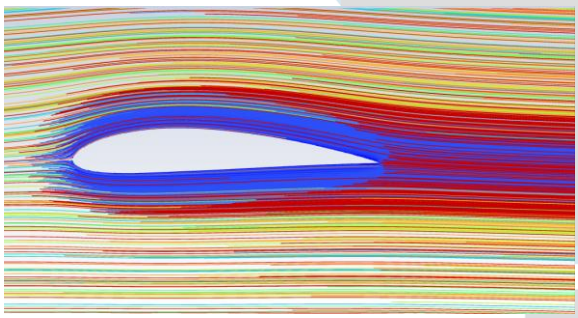

**Fig. 9:(a)** Flow field of NACA 4415 at 0° AoA

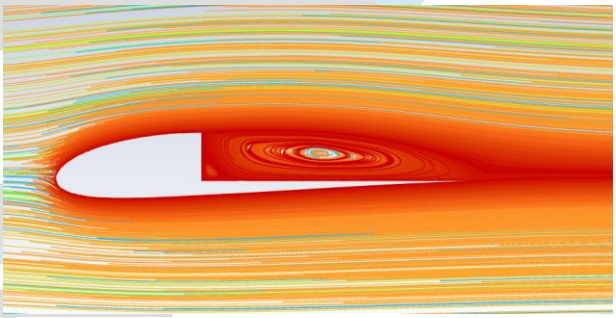

**Fig. 9:(b)** Flow field of KFm-2 airfoil at 0° AoA showing the initiation of recirculation

At 16°, these effects intensify. The upper surface shows a larger low-pressure region and a well-defined recirculation zone with steep velocity gradients. In contrast, for a NACA 4415 airfoil at similar angles, pressure contours become irregular beyond 60–70% chord, indicating strong adverse pressure gradients and flow separation. Velocity contours show a large low-speed region forming near the trailing edge and rapidly extending upstream, with loss of the high-velocity region over the upper surface, confirming stall onset. However, in the KFm airfoil, the step anchors the separation, preventing its upstream movement and avoiding abrupt stall. The wake becomes more pronounced but remains structured.

## IV. CONCLUSIONS

The present study provides a detailed comparative aerodynamic evaluation of the NACA 4415 and KFm-2 airfoils, focusing on lift characteristics and stall behavior across subsonic Mach numbers ranging from 0.3 to 0.6 and angles of attack from 0° to 16°. The results indicate that the NACA 4415 airfoil demonstrates superior lift generation in the pre-stall region, achieving higher lift coefficients at lower angles of attack due to its cambered geometry and efficient aerodynamic design. However, this advantage is limited by an earlier onset of stall, typically around 12°, beyond which the airfoil experiences a noticeable drop in lift. This behavior is attributed to the inability of the boundary layer to withstand the increasing adverse pressure gradient at higher angles

of attack, leading to rapid flow separation and a sharp degradation in performance. In contrast, the KFm-2 airfoil exhibits a fundamentally different aerodynamic behavior characterized by delayed stall and improved performance at higher angles of attack. Although it produces comparatively lower lift coefficients at smaller angles, the lift values achieved by the NACA 4415 at lower angles are progressively attained by the KFm-2 airfoil at higher angles of attack. This indicates that while the initial lift generation is lower, the KFm-2 compensates through sustained lift production over an extended range of angles. The absence of a sharp decline in lift up to 16° demonstrates its ability to maintain aerodynamic effectiveness even beyond the typical stall angle of conventional airfoils. The lift curve trends further emphasize this distinction, where both airfoils exhibit nearly linear behavior in the pre-stall region with similar lift curve slopes, indicating comparable sensitivity to angle of attack initially. However, the divergence becomes evident at higher angles, where the NACA 4415 reaches its peak and begins to lose lift, whereas the KFm-2 continues to show a steady increase without significant degradation. This highlights that the key difference between the two airfoils lies not in their initial lift-generating capability, but in their post-critical performance and stall characteristics.

Additionally, the aerodynamic performance of both airfoils remains relatively consistent across the tested Mach number range, indicating minimal compressibility effects within the subsonic regime. The KFm-2 airfoil, in particular, shows stable lift characteristics across all Mach numbers, suggesting robustness and reliability under varying operating conditions. While the maximum lift coefficient of the NACA 4415 is higher, the KFm-2 demonstrates a more gradual and controlled approach to stall, which is a significant advantage in applications requiring high-angle operation and enhanced stability.

Overall, the study concludes that while the NACA 4415 airfoil is better suited for conditions requiring high lift at lower angles of attack, the KFm-2 airfoil offers superior performance in terms of stall delay and lift sustainability at higher angles. The ability of the KFm-2 to achieve comparable lift values at elevated angles, combined with its resistance to abrupt stall, makes it a promising alternative for applications such as unmanned aerial vehicles, low-speed aircraft, and other systems where aerodynamic stability and extended operational range are critical.

## REFERENCES

[1] Kabir, A., Akib, Y. M., Hasan, M., & Islam, Md. J. (2021). *Comparison of the aerodynamic performance of NACA 4415 and KFm based stepped airfoils*. 040003. https://doi.org/10.1063/5.0037582

[2] Kabir, A., Islam, M., Jahan, N., Akib, Y. M., & Mili, M. I. J. (2021). Numerical Simulation and Comparative Study of Aerodynamic Performance of Kline Fogleman Modified Backward Stepped Airfoils and the NACA 4415 Airfoil. *SSRN Electronic Journal*. https://doi.org/10.2139/ssrn.3819496

[3] T. Cebeci and P. Bradshaw, *Momentum Transfer in Boundary Layers*. New York, USA: McGraw-Hill, 1977.

[4] M. Gad-el-Hak, "Flow separation control," *Applied Mechanics Reviews*, vol. 49, no. 6, pp. 365–379, 1996.

[5] P. G. Huang and C. J. Yang, "A review of laminar separation bubble control," *Progress in Aerospace Sciences*, vol. 37, no. 7, pp. 633–682, 2001.

[6] J. D. Anderson, *Fundamentals of Aerodynamics*, 5th ed. New York, USA: McGraw-Hill, 2010.

[7] M. S. Selig, J. J. Guglielmo, A. P. Broeren, and P. Giguère, *Summary of Low-Speed Airfoil Data*. SoarTech Publications, 1995.

[8] Wygnanski, I., & Champagne, F. (1973). On transition in a separated laminar boundary layer. *Journal of Fluid Mechanics*, 59(2), 281–335. https://doi.org/10.1017/S0022112073001575

[9] Gaster, M. (1967). The structure and behaviour of laminar separation bubbles. *Aeronautical Quarterly*, 18(2), 163–175. https://doi.org/10.1017/S0001925900004383

[10] Greenblatt, D., & Wygnanski, I. J. (2000). The control of flow separation by periodic excitation. *Progress in Aerospace Sciences*, 36(7), 487–545. https://doi.org/10.1016/S0376-0421(00)00008-7

[11] Schlichting, H., & Gersten, K. (2017). *Boundary-Layer Theory* (9th ed.). Springer. https://doi.org/10.1007/978-3-662-52919-5

[12] Thwaites, B. (1949). Approximate calculation of the laminar boundary layer. *Aeronautical Quarterly*, 1, 245–280. https://doi.org/10.1017/S0001925900000188

[13] Drela, M. (1989). XFOIL: An analysis and design system for low Reynolds number airfoils. In *Low Reynolds Number Aerodynamics*. Springer. https://doi.org/10.1007/978-3-642-84010-4_1

[14] McGhee, R. J., & Beasley, W. D. (1973). Low-speed aerodynamic characteristics of a 14-percent thick airfoil section. *NASA Technical Report*. https://doi.org/10.2514/6.1973-123

[15] Bradshaw, P. (1973). Effects of streamline curvature on turbulent flow. *AGARDograph*. https://doi.org/10.2514/5.9781600866447

[16] Simpson, R. L. (1989). Turbulent boundary-layer separation. *Annual Review of Fluid Mechanics*, 21, 205–232. https://doi.org/10.1146/annurev.fl.21.010189.001225

[17] Yarusevych, S., Sullivan, P. E., & Kawall, J. G. (2009). On vortex shedding from an airfoil in low-Reynolds-number flows. *Journal of Fluid Mechanics*, 632, 245–271. https://doi.org/10.1017/S0022112009007058

[18] Wu, J. Z., Ma, H. Y., & Zhou, M. D. (2006). *Vorticity and Vortex Dynamics*. Springer. https://doi.org/10.1007/978-3-540-30728-5

[19] Spalart, P. R., & Allmaras, S. R. (1992). A one-equation turbulence model for aerodynamic flows. *AIAA Paper 92-0439*. https://doi.org/10.2514/6.1992-439